ACS Photonics

pubs.acs.org/journal/apchd5

Article

Optical Third-Harmonic Generation in Hexagonal Boron Nitride Thin Films

Anna A. Popkova, Ilya M. Antropov, Johannes E. Fröch, Sejeong Kim, Igor Aharonovich, Vladimir O. Bessonov,* Alexander S. Solntsev, and Andrey A. Fedyanin

Cite This: *ACS Photonics* 2021, 8, 824–831

Read Online

ACCESS | Metrics & More | Article Recommendations | Supporting Information

ABSTRACT: Hexagonal boron nitride (hBN) is a layered material that exhibits remarkable optical features in the UV, visible, and IR ranges, attractive for applications in modern photonics. Being transparent in a wide spectral range, hBN is now considered an important building block for novel integrated photonic platforms, thus requiring the study of its optical properties. In this work, we report on the measurements of hBN optical cubic nonlinearity $\chi^{(3)}$ equal to 8.4×10^{-21} m^2/V^2 by observing the third-harmonic generation for 1080 nm pump wavelength from mechanically exfoliated hBN flakes with thicknesses varying from 5 to 170 nm. The third-order susceptibility of hBN is close to that of Si_3N_4 highlighting the potential of hBN for nonlinear applications.

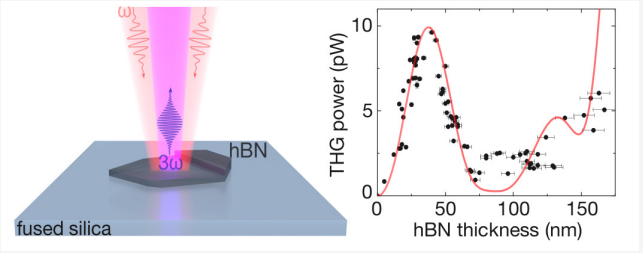

KEYWORDS: *hexagonal boron nitride, third-harmonic generation, third-order susceptibility, 2D materials, coherence length, nonlinear optics*

Hexagonal boron nitride (hBN), graphene, transition metal dichalcogenides (TMDCs), and their hybrid systems are several examples of 2D materials attracting great attention due to their unique electronic and optical properties, such as tunable band gap,[1] ultrafast carrier dynamics,[2,3] bright photoluminescence,[4] and saturable absorption.[5] While most 2D materials are metals or semiconductors, hBN is a dielectric with a large band gap of approximately 6 eV.[6,7] This material possesses high optical transparency in the visible spectrum,[8] high mechanical strength,[9] chemical and thermal stability, and excellent oxidation resistivity.[10] hBN has a graphene-like crystal structure and a smooth surface free of charge traps and dangling bonds,[11] which determine its widespread use as an excellent insulating substrate for graphene-based electronic and optoelectronic devices[12−15] as well as an encapsulating layer for other 2D materials.[16−18] Moreover, the discovery in the past few years of new optical properties of hBN has led to the consideration of this material as a standalone photonic platform. hBN has been shown to support hyperbolic polaritons in the mid-IR,[19] demonstrate strong luminescence in the deep-UV,[6,8] and exhibit bright single-photon emission in the visible and mid-IR from point defects.[20] Techniques of fabricating large-area hBN films with a thickness of units to hundreds nanometers, together with methods of their structuring, have also evolved dramatically[21] paving the way to hBN-based integrated photonics. As the first clear examples, 1D and 2D photonic crystal cavities made of hBN and Si_3N_4/hBN were recently demonstrated to enhance the emission of single photons from the defects inside the cavities.[22,23]

Determining the hBN nonlinear optical constants is the next essential step toward understanding the capabilities of hBN photonics. Most of the research has been limited so far to the study of quadratic nonlinearity of hBN. Second-harmonic generation (SHG) from hBN monolayer showed the polarization dependence linked to the crystallographic axes and gave the value of the surface nonlinear susceptibility comparable with that of highly nonlinear crystals such as lithium niobate.[24] However, with an increase of the number of hBN layers, each pair of layers forms a centrosymmetric structure leading to the elimination of SHG in hBN of even layer thickness.[24,25] This makes SHG very sensitive to the number of hBN layers but, for the case of thick hBN films, limits the second-harmonic intensity to that obtained from a single layer.[26] Due to inversion symmetry, third-harmonic generation (THG) should be comparable with or dominate over SHG with increasing film thickness, making THG prospective for application in hBN photonics transparent in the wide spectral range. Knowing the cubic nonlinearity of hBN is essential for its

Received: November 17, 2020
Published: February 24, 2021

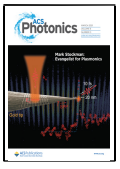

use both as a material in integrated optics and as a substrate or encapsulating layer in photonics based on graphene[27] and other 2D materials.[28]

Third-order nonlinear processes in hBN have not been studied before. In this work, we fill this gap by measuring THG in hBN flakes of various thicknesses in the range from 5 to 170 nm. The flakes are mechanically exfoliated from the hBN crystal by the method enabling the preparation of thick hBN films suitable for photonics applications.[29] Using several methods, we estimate the value of hBN cubic nonlinear susceptibility, which appears to be comparable with the cubic susceptibility of Si_3N_4.

EXPERIMENTAL METHODS

THG in hBN flakes was measured using a home-built multiphoton microscope shown in Figure 1. The laser beam

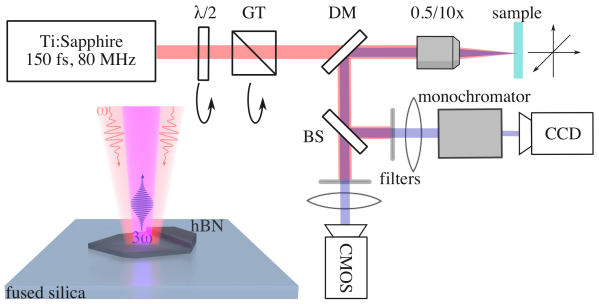

Figure 1. Schematic of the experimental setup. $\lambda/2$ is achromatic half-wavelength plate, GT is Glan−Tailor prism, DM is dichroic mirror, BS is beam splitter.

of Ti:sapphire femtosecond laser (Coherent Chameleon Ultra 2, tuning range 680−1080 nm, 80 MHz repetition rate, 150 fs pulse duration) passed through a half-wave plate on a motorized rotational stage and Glan−Tailor prism, which controlled the power and polarization of the pump radiation. Then the beam was focused by an objective lens (NA = 0.5, 10×) to a 3-μm spot at the surface of the sample mounted on a 3-axis motorized stage (SigmaKoki). The nonlinear radiation reflected from the sample was collected by the same objective lens and directed by a dichroic mirror (DMLP650, Thorlabs) to the detection channel consisted of two arms. The first arm, comprising a set of short-pass filters (1 FGB37 Thorlabs filter, 4 FGUV11 Thorlabs filters), a tube lens (ACA254-100-UV Thorlabs), and a cooled CMOS camera (Photometrics Prime BSI), was used for third-harmonic (TH) intensity mapping. The second arm was employed to measure the spectrum of nonlinear signal and composed of a filter (FGB39 Thorlabs), a tube lens (ACA254-150-UV Thorlabs), and a monochromator (Solar M150, 1200 lp/mm) combined with a CCD camera (Andor Clara). The experimental setup was fully automated. The TH intensity maps were measured at the pump wavelength of 1080 nm in order to minimize absorption of TH radiation in the setup optical elements.

The sample is a set of layered hBN flakes prepared on the fused silica substrate by the method previously developed for transition metal dichalcogenides[30] and adopted for hBN (see Methods for details). The thickness maps of hBN flakes were measured using an atomic force microscope (AFM) (NT-MDT NTEGRA) working in a semicontact mode. The size of the probe tip was approximately 10 nm.

RESULTS AND DISCUSSION

Optical image of a typical hBN flake is shown in Figure 2 (a). The sample has areas of various colors caused by light interference in a thin film. Figure 2 (b) demonstrates the AFM image of the flake revealing its average thickness of approximately 160 nm (Figure S3). The full thickness range for studied hBN flakes is from 5 to 170 nm. The intensity map of the TH radiation reflected from the flake is displayed in Figure 2 (c). THG map was obtained with the 30 mW pump power by scanning the sample in increments of 1 μm. The area with high intensity has the shape of the flake. The TH signal from the flake region is 3 orders of magnitude higher than the signal from the fused silica substrate. This indicates that the value of cubic susceptibility of hBN is at least an order of magnitude higher than that of fused silica.

The spectra of nonlinear-optical signal and its dependence on the pump power were measured to confirm the nature of the observed nonlinear process. The signal was collected from homogeneous area with 60 nm thickness in the center of the flake to avoid the edge effect. Figure 3 (a) depicts a set of THG spectra measured at various powers of the pump radiation with the central wavelength of 1080 nm. The THG spectra line width of about 4 nm is more than 3 times smaller than the pump spectrum line width (see Figure S1), which agrees with the theory[31] taking into account 0.8 nm spectral resolution of the setup. We also measured the spectrum of the nonlinear signal with the set of filters used in front of the CMOS camera in the first detection arm. The spectrum (Figure S2) does not contain any features, such as luminescence or second-harmonic generation, in the trans-

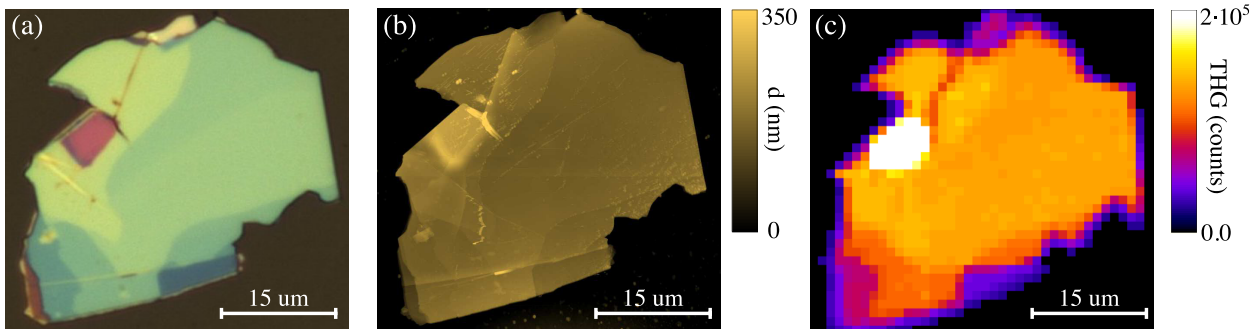

Figure 2. Images of a typical hBN flake. (a) Optical image. (b) AFM image. The average thickness is approximately 160 nm. (c) TH intensity map. The intensity of THG from hBN is 3 orders of magnitude higher than that from fused silica substrate.

https://dx.doi.org/10.1021/acsphotonics.0c01759
ACS Photonics 2021, 8, 824−831

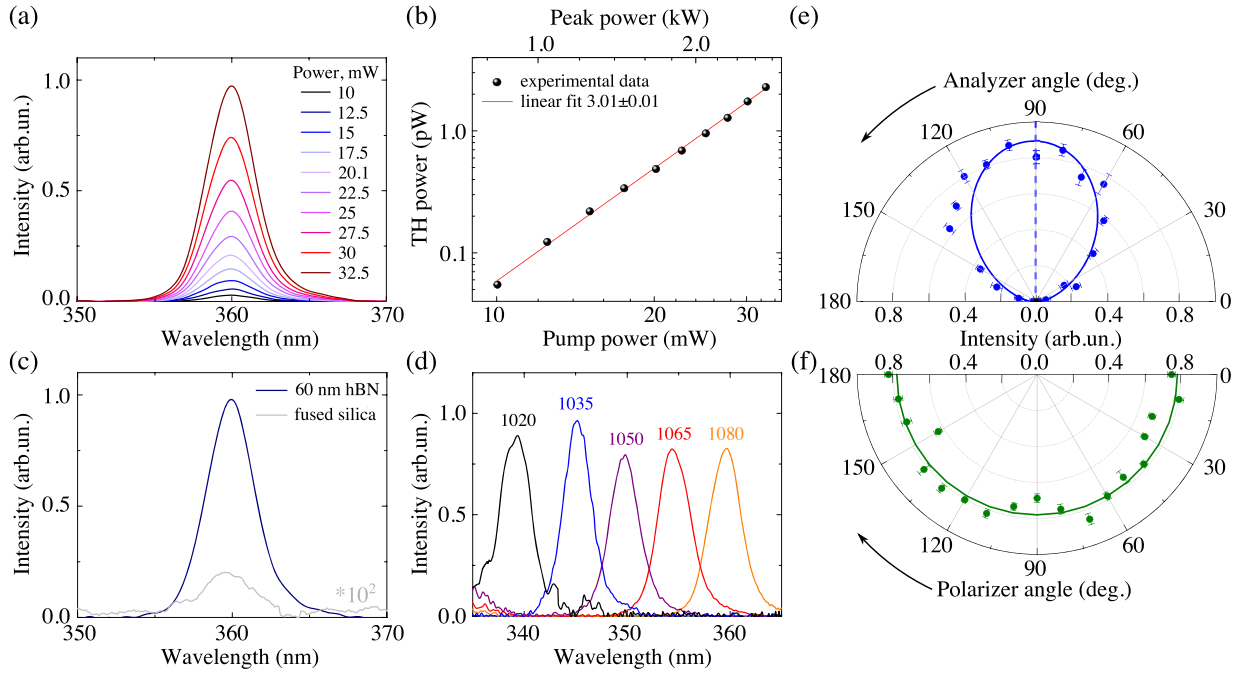

Figure 3. THG from hBN flakes. (a) Spectra of the THG signal from the 60 nm-thick hBN flake depending on the pump radiation power. (b) THG power dependence. (c) Spectra of THG signals from the hBN flake and fused silica substrate measured at 30 mW pump power. (d) Spectra of the THG signal from the hBN flake for various pump wavelengths. (e) Dependence of the THG signal on the analyzer angle. A blue curve shows $cos^2(\phi)$ dependence corresponding to the Malus' law for polarization direction of the linearly polarized pump radiation, shown by a blue dashed line. (f) THG signal depending on the polarization direction of the pump radiation. A green curve shows a constant value corresponding to the average THG signal.

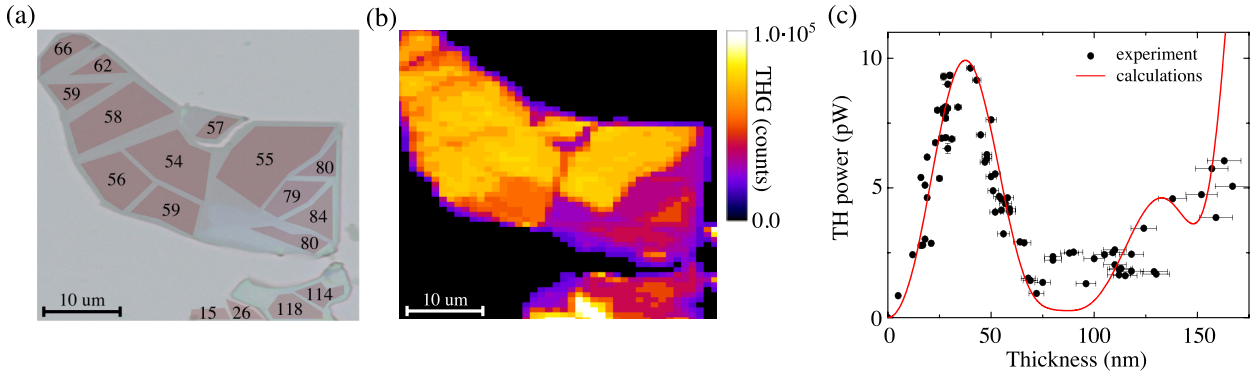

Figure 4. THG dependence on the hBN thickness. (a) Optical image of the flake with a thickness map overlaid on top. The numbers correspond to the flake thickness in nanometers. (b) TH intensity map of the hBN flake. (c) Dependence of the THG power on the hBN thickness. Experimental data are shown with black dots. Numerical data obtained by nonlinear transfer matrix method are shown with red curve.

mission window of the filters, indicating that only THG was measured in the mapping experiments. Figure 3(b) shows the log−log plot of the THG power versus the power of the pump radiation incident on the sample. The values of the THG power were obtained by carefully converting the number of TH counts acquired from the CMOS camera taking into account the transmission of all optical elements (see Methods for details). The signal power follows the expected cubic dependence on the pump power, the log−log plot shows a linear slope of 3.01 ± 0.01. The spectral measurements for fused silica substrate performed at 30 mW pump power demonstrate the TH signal with intensity of almost 3 orders of magnitude less than one from the hBN flake (Figure 3 (c)), which is consistent with THG mapping experiments. We also obtained the TH spectra at various pump wavelengths close to 1080 nm. The results in Figure 3 (d) show that there is no strong spectral dependence of THG in the studied wavelength range, as is expected for pump and third-harmonic photon energies below the hBN bandgap.

The polarization of the TH radiation was measured by rotating an analyzer (Glan−Tailor prism) set between the dichroic mirror and the beam splitter into the detection channel. Figure 3 (e) shows the experimental dependence (dots) and the result of approximation by Malus' law (blue curve) with the polarization direction of the pump radiation (dashed line). A good agreement between experiment and theory reveals that TH radiation is linearly polarized along the polarization of the fundamental beam. The TH intensity dependence on the angle between the pump polarization and a crystallographic axis of hBN was also checked by rotating the Glan−Tailor prism placed in the pump channel between the dichroic mirror and the objective lens. Figure 3 (f)

https://dx.doi.org/10.1021/acsphotonics.0c01759
ACS Photonics 2021, 8, 824−831

demonstrates that the TH intensity for various polarizer angles is approximately constant, i.e., THG independent of the hBN azimuthal angle. This result is typical for all crystals belonging to the D_{6h} point group of symmetry.[32,33]

The determination of the TH intensity dependence on the thickness of hBN film is necessary to estimate correctly the third-order susceptibility. First, flakes with homogeneous areas of various thicknesses were selected using optical microscopy and AFM. An example of an optical image of the flake with its thickness map superimposed on top is shown in Figure 4 (a). Then, the TH intensity maps of the flakes were measured (Figure 4 (b)) and compared with the corresponding thickness maps to find the coordinates of points related to the flake areas with a constant thickness. For these points, time dependence of the TH signal was measured for 2 min at the pump power of 30 mW. The THG time dependence close to the constant during the measurement guaranteed that there was no undesirable hBN degradation and influence of edge effects or focus shifts. By averaging obtained TH intensity values for each flake point with known thickness, the THG thickness dependence was revealed (Figure 4 (c)). We found that the TH intensity varies non-monotonically with increasing hBN film thickness.

Unlike SHG in hBN produced by a single layer due to the inverse symmetry of the hBN volume,[26] TH is generated in the entire volume of the medium. Thus, the total reflected TH wave is the result of the interference of TH waves generated in the hBN volume in the direction opposite to the propagation direction of the pump waves. For a semi-infinite media, the phase shift of the reflected TH wave generated in the layer at a distance d from the surface is the sum of the $3k_\omega d$ phase shift of the forward propagating source wave and the $k_{3\omega}d$ phase shift of the backward propagating free TH wave, where k_ω and $k_{3\omega}$ are the wave vectors of light at frequencies corresponding to the subscript. From here, by analogy with classical theory of forward harmonic generation, one can determine the coherence length L_{coh}, for which the phase of the reflected TH wave shifts by π. This means that the intensity of TH reflected from a thin film reaches a maximum at a film thickness of approximately L_{coh}. For hBN, $L_{coh} = \lambda/6(n^{\omega}_{hBN} + n^{3\omega}_{hBN}) = 45$ nm, where $\lambda = 1080$ nm is the pump wavelength, $n^{\omega}_{hBN} = 1.9$ and $n^{3\omega}_{hBN} = 2.1$[34] are refractive indexes of hBN for pump and harmonic wavelengths, respectively.

With a further increase in the film thickness, TH waves generated in deeper layers begin to interfere destructively with waves generated in layers close to the surface leading to the decrease in the detected TH intensity. The minimum intensity is reached for a film thickness of $2L_{coh} = 90$ nm, which is in good agreement with Figure 4 (c). However, in the case of a film, we must take into account the influence of the second interface (hBN/substrate in our case) on the positions of maxima and minima in the THG thickness dependence, which is caused by two mechanisms. The first one is modifying the source wave due to multiple reflected fundamental waves leading to contributions at the fundamental frequency to the source wave.[35] The second mechanism is associated with the forward-generated TH wave reflected from the hBN/substrate interface, which interferes with backward propagating TH waves generated in the hBN volume. These effects explain both the shift of the first TH intensity maximum (observed at 37 nm in Figure 4 (c)) toward the film thicknesses less than L_{coh}, and the complication of the THG thickness dependence. The influence of all waves is taken into account in the simulation of the THG thickness dependence using well-known nonlinear transfer matrix method[35,36] applied to study the nonlinear optical response of multilayer structures.[37,38] The numerical results are shown by red curve in Figure 4 (c) demonstrating a good agreement with experimental dependence. We varied the value of hBN third-order susceptibility $\chi^{(3)}$ to obtain the amplitude of the calculated and experimental TH signal equal to each others for hBN thickness in the vicinity of 37 nm (see Methods for details). We determine the hBN susceptibility $\chi^{(3)} = (8.4 \pm 0.5) \times 10^{-21}$ m^2/V^2. Note that the found $\chi^{(3)}$ is a combination of in-plane components of the cubic susceptibility tensor of hBN, since the contribution of out-of-plane components is expected to be negligible under our experimental conditions (see Methods for details).

The susceptibility value can also be estimated by comparing the intensities of THG from hBN and the fused silica substrate measured under the same experimental conditions. Very thin films can be considered as nonlinear sheets with cubic susceptibility $\chi^{(3)}_s$. The theory of harmonic generation by a nonlinear monolayer gives an analytical expression for the harmonic power[39] and allows us to determine the susceptibility from the experimentally obtained harmonic power. For films with thicknesses $d \ll L_{coh}$ at which the effects of the phase shift of the pump and harmonic waves are negligible, the bulk susceptibility of the film material can be obtained as $\chi^{(3)} = \chi^{(3)}_s/d$.[40] In turn, an analytical formula for the power of TH reflected from a semi-infinite medium, which is the case of a substrate, is given by Bloembergen.[41] Thus, considering the ratio of the THG powers measured from the 5 nm-thick hBN flake and from the fused silica substrate and taking into account the fused silica susceptibility from ref 42, we obtain the hBN cubic susceptibility $\chi^{(3)} = (4.8 \pm 0.5) \times 10^{-21}$ m^2/V^2 (see Methods for details). This value gives a lower estimate for the susceptibility, does not depend on the parameters of the experiment, and close to the previous value obtained by the nonlinear transfer matrix method.

Finally, we present in Table 1 a comparison of the hBN cubic susceptibility with the susceptibilities of two groups of materials—well-studied two-dimensional materials and popular materials in integrated photonics. Note that, in our case, the energies of the pump and third harmonic photons are lower than the band gap of hBN, implying that the susceptibility is obtained for the nonresonant case. Therefore, it is correct to compare the susceptibilities measured in the nonresonant case for other two-dimensional materials. However, little research has been done on the cubic nonlinearity of popular 2D

Table 1. Typical Cubic Susceptibilities Obtained by the THG Method for 2D and Other Materials Commonly Used in Photonics

material	$\chi^{(3)} \times 10^{-20}$, m^2/V^2	λ_ω, nm	ref
hBN	0.84	1080	
graphene	20	800	45
$MoSe_2$	22	1560	46
MoS_2	0.01	2000	43
WSe_2	10	1560	46
WS_2	24	1560	46
Si	260	1060	47
GaAs	200	1060	47
Si_3N_4	2.8	1064	48
fused silica	0.02	1064	42

https://dx.doi.org/10.1021/acsphotonics.0c01759
ACS Photonics 2021, 8, 824−831

materials so far, with susceptibility values varying over several orders of magnitude as can be seen from the extended Table S1 in the Supporting Information. A reliably nonresonant value of 10^{-22} m^2/V^2 can be given only for MoS_2.[43] For the rest of the dichalcogenides we give the values only for the longest pump wavelengths, when the one- and two-photon transitions are nonresonant. In the last cases the hBN cubic susceptibility is an order of magnitude lower than that of dichalcogenides. Graphene has no band gap, and we show its cubic susceptibility for the pump wavelength close to that from our experiment. On the other hand, the susceptibility of hBN is 2 orders of magnitude lower than the cubic susceptibility governing THG in popular materials for waveguides—Si and GaAs—at the pump wavelength close to 1080 nm. As in the case of the above experiments on THG in 2D materials, the energy of three-photon transitions exceeds the band gap of Si and GaAs, which leads to an increase in the susceptibility due to the presence of real electron transitions. Moreover, the energy of three-photon transitions for Si corresponds to the energy of direct electronic transitions (~3.45 eV) in the region of the Γ point,[44] meaning that the Si cubic susceptibility has a resonance at a pump wavelength in the vicinity of 1080 nm. However, for the same reason, the applicability of these materials is limited to the infrared range. The closest in parameters to hBN is silicon nitride, which is actively used in integrated photonics. We note that the hBN susceptibility is comparable to that of silicon nitride, which confirms the possibility of using hBN for nonlinear optical applications.

In conclusion, we have observed THG reflected from mechanically exfoliated hBN flakes with thicknesses from 5 to 170 nm. The TH radiation is linearly polarized along the polarization of the pump radiation and shows isotropic azimuthal dependence. We revealed non-monotonous THG dependence on the hBN flake thickness demonstrating an intensity peak at a film thickness of 37 nm, which is the result of phase-matched THG together with interference of multiple reflected TH waves. By simulating the THG thickness dependence, as well as by directly comparing the THG from fused silica and hBN, we evaluated the hBN susceptibility $\chi^{(3)} = (8.4 \pm 0.5) \times 10^{-21}$ m^2/V^2. The obtained value is an order of magnitude less than the resonance cubic susceptibilities of TMDCs and is comparable to the susceptibility of silicon nitride, which is a popular material for integrated photonics operating in a wide spectral range. We note that, due to a sufficiently high susceptibility, the THG can be used to characterize thin (down to a few layers) hBN films and estimate their thicknesses regardless of the parity of the number of layers, which is critical for the case of second-harmonic generation.

METHODS

hBN Exfoliation. Crystalline hBN flakes were deposited and cleaved several times on a sticky tape. The top surface was coated with a 50 nm gold film using sputter deposition. A thermal release tape was used to exfoliate the hBN/gold film. The tape was stuck onto a fused silica substrate, which was treated with O_2 plasma to increase the adhesion. Then the tape was released using a hot plate, leaving the gold film on top of hBN intact. The substrate was cleaned using piranha acid, followed by the further UV-Ozone treatment. The gold layer was then removed using aqua regia. Thin hBN flakes were put on the final target substrate using the standard wet transfer technique. At the end, the PMMA layer was removed using a warm acetone bath and UV ozone treatment.

Determination of THG Power. The THG power was obtained from measurements carried out with the CMOS camera (Figure 1). We converted TH counts to light power and measured transmittance of all optical elements using the second-harmonic radiation generated by 720 nm pump pulses in a β-barium borate crystal. The conversion coefficient for the CMOS camera was determined by measuring the number of counts generated by a 360 nm-wavelength signal of a given power. As a verification of the accuracy of our measurements, transmittance of experimental setup elements were calculated using the appropriate datasheets. The result values of conversion for two cases were very close to each other.

Calculation of THG Thickness Dependence. Nonlinear transfer matrix method[35] is used to calculate THG in multilayer structure taking into account all reflections of pump and harmonics waves from the interfaces and the phase shifts of all waves. In our case, the calculated structure consisted of an hBN layer placed between two semi-infinite layers of air and fused silica. The refractive indexes of hBN for the pump and TH wavelengths were 1.9 and 2.1,[34] respectively. The refractive indexes of the fused silica substrate are 1.45 and 1.47[49] for the pump and TH wavelengths, respectively. The cubic nonlinear susceptibility of the substrate was considered negligible. The calculation of the THG thickness dependence was carried out for an average pump power of 30 mW, corresponding to that in the experiment. First, the peak intensity of the pump radiation was found for the experimental parameters of the laser pulse and the waist size of the pump radiation, from which the pump electric field was determined.[50] Next, we calculated the dependence of the field strength of the TH wave propagating back into air on the hBN film thickness. Finally, the TH field was converted back to TH average power taking into account the reduced TH pulse duration and beam diameter.[51] By varying the value of the hBN cubic susceptibility, the calculated value of the THG power for a film thickness of 37 nm was adjusted to the experimental one.

Estimation of $\chi^{(3)}$ Using Reference Sample. The fused silica substrate was used as a reference sample for THG measurements. In our case, the pump radiation is focused with a low numerical aperture (NA = 0.22), and the TH field reflected from a semi-infinite nonlinear medium can be calculated using the formula for normal incidence:[41]

$$E(3\omega) = \frac{P_{NL}^{(3)}}{\epsilon_0 (n_1^{\omega} + n_2^{\omega})(n_2^{\omega} + n_2^{3\omega})} \quad (1)$$

where $P_{NL}^{(3)}$ is cubic polarization, n_1 and n_2 are refractive indexes of air and fused silica, respectively, at the frequencies corresponding to the superscripts. For the THG process, $P_{NL}^{(3)} = \epsilon_0 \chi^{(3)} E^3(\omega)$, where $E(\omega)$ is the pump field in the nonlinear medium. Finally, the equation for the average power of TH reflected from fused silica is

$$P(3\omega)_{SiO_2} = \frac{64 S^2 |\chi^{(3)}|^2_{SiO_2} (n_1^{\omega})^4 P^3(\omega)}{3\sqrt{3}\,(\epsilon_0 c \pi r^2 f \tau)^2 (n_1^{\omega} + n_2^{\omega})^8 (n_2^{\omega} + n_2^{3\omega})^2} \quad (2)$$

where c is speed of light, ϵ_0 is permittivity of free-space, f = 80 MHz is the pulse repetition rate, τ = 150 fs is the pulse duration, r = 1.5 μm is the focal spot radius, S = 0.94 is the

https://dx.doi.org/10.1021/acsphotonics.0c01759
ACS Photonics 2021, 8, 824−831

shape factor for Gaussian pulses, $P(\omega)$ = 30 mW is the pump radiation power, $|\chi^{(3)}|_{SiO_2}$ = 2.2 × 10^{-22} m^2/V^2 is the nonlinear susceptibility of fused silica,[42] n_2^{ω} = 1.45 and $n_2^{3\omega}$ = 1.47 are refractive indexes of fused silica[49] and n_1 = 1 is the refractive index of air. We calculated the THG power of 25 fW, which is very close to the experimental value of 32 ± 5 fW.

The formula for nonlinear optical susceptibility of extremely thin films can be found by the method described in ref 51. For known pump $P(\omega)$ and TH $P(3\omega)_{hBN}$ powers, the nonlinear susceptibility $|\chi_s^{(3)}|$ of polarization sheet can be calculated as

$$|\chi_s^{(3)}| = \sqrt{\frac{P(3\omega)_{hBN}}{P^3(\omega)} \frac{c^2 \epsilon_0^2 f^2 \tau^2 r^4 \lambda^2 (1 + n_2^{\omega})^8}{256\sqrt{3} S^2}} \quad (3)$$

where λ = 1080 nm is the laser wavelength. In the case of a film thickness $d \ll L_{coh}$, when the harmonic power quadratically depends on the film thickness, the hBN bulk susceptibility is $|\chi^{(3)}|_{hBN} = \frac{|\chi_s^{(3)}|}{d}$.

The expression for hBN cubic susceptibility $|\chi^{(3)}|_{hBN}$ is obtained from eq 2 and eq 3:

$$|\chi^{(3)}|_{hBN} = \frac{\lambda}{6\pi d(n_2^{\omega} + n_2^{3\omega})} \sqrt{\frac{P(3\omega)_{hBN}}{P(3\omega)_{SiO_2}}} |\chi^{(3)}|_{SiO_2} \quad (4)$$

The result value of nonlinear optical susceptibility of hBN obtained by this method from 5 nm flake is $\chi^{(3)}$ = (4.8 ± 0.3) × 10^{-21} m^2/V^2.

hBN $\chi^{(3)}$ Components. The hBN volume has a D_{6h} point group symmetry.[32] For this crystal lattice, the third-order nonlinear susceptibility tensor has 21 nonzero components satisfying the following relations:

$$\begin{cases} \chi^{(3)}_{xxxx} = \chi^{(3)}_{yyyy} = 3\chi^{(3)}_{xxyy} = 3\chi^{(3)}_{yxxy} \\ \chi^{(3)}_{xxzz} = \chi^{(3)}_{yyzz} \\ \chi^{(3)}_{zzzz} \\ \chi^{(3)}_{zxxz} = \chi^{(3)}_{zyyz} \end{cases} \quad (5)$$

where the terms are invariant under permutations of the last three indices.[52] We can distinguish in-plane components of the $\chi^{(3)}$ tensor, which have only x and y indices, and out-of-plane components that have z indices. The experimental conditions correspond to the case of weak focusing of the pump radiation incident on the sample. The focusing numerical aperture is NA = 0.22, which corresponds to a maximum angle of incidence of 11 degrees in air, or approximately 6 degrees in the hBN volume. Thus, the ratio of the in-plane and out-of-plane components of the pump radiation field can be roughly estimated as $E_x/E_z \sim 10$. If we assume that all the susceptibility tensor components are comparable to each other, the contribution to TH signal from out-of-plane components will be at least 2 orders of magnitude smaller (the case of $\chi^{(3)}_{zxxz}$) than the contribution from in-plane components.

In the experiment, the energies of pump and TH photons are far below the energies of resonance transitions in hBN, i.e., the medium is transparent and has low dispersion. This allows us to estimate the ratio between in-plane and out-of-plane tensor components using Miller's rule,[53] expressing $\chi^{(3)}$ in terms of the product of the corresponding components of the linear susceptibility $\chi^{(1)}$. In accordance with the literature,[54,55] and taking into account the anisotropy of the hBN refractive index,[34] we find

$$\frac{\chi^{(3)}_{xxxx}}{\chi^{(3)}_{zzzz}} = \frac{\chi^{(1)}_{xx}(3\omega)(\chi^{(1)}_{xx}(\omega))^3}{\chi^{(1)}_{zz}(3\omega)(\chi^{(1)}_{zz}(\omega))^3} \approx 20 \quad (6)$$

Thus, we expect that the contribution of the out-of-plane components of the hBN cubic susceptibility is negligible and only the combination of the in-plane components was measured in the experiment.

■ ASSOCIATED CONTENT

Supporting Information

The Supporting Information is available free of charge at https://pubs.acs.org/doi/10.1021/acsphotonics.0c01759.

Spectrum of the pump radiation; spectrum of the nonlinear signal; THG, optical and AFM images of various hBN flakes; extended table with cubic susceptibilities of 2D materials (PDF)

■ AUTHOR INFORMATION

Corresponding Author

Vladimir O. Bessonov − *Faculty of Physics, Lomonosov Moscow State University, Moscow 119991, Russia; Frumkin Institute of Physical Chemistry and Electrochemistry, Russian Academy of Sciences, Moscow 119071, Russia;* orcid.org/0000-0002-2165-1924; Email: bessonov@nanolab.phys.msu.ru

Authors

Anna A. Popkova − *Faculty of Physics, Lomonosov Moscow State University, Moscow 119991, Russia;* orcid.org/0000-0002-4758-6833

Ilya M. Antropov − *Faculty of Physics, Lomonosov Moscow State University, Moscow 119991, Russia*

Johannes E. Fröch − *School of Mathematical and Physical Sciences, University of Technology Sydney, Ultimo, New South Wales 2007, Australia;* orcid.org/0000-0003-1111-9704

Sejeong Kim − *Department of Electrical and Electronic Engineering, University of Melbourne, Melbourne, Victoria 3010, Australia;* orcid.org/0000-0001-9836-3608

Igor Aharonovich − *School of Mathematical and Physical Sciences and ARC Centre of Excellence for Transformative Meta-Optical Systems (TMOS), University of Technology Sydney, Ultimo, New South Wales 2007, Australia;* orcid.org/0000-0003-4304-3935

Alexander S. Solntsev − *School of Mathematical and Physical Sciences, University of Technology Sydney, Ultimo, New South Wales 2007, Australia;* orcid.org/0000-0003-4981-9730

Andrey A. Fedyanin − *Faculty of Physics, Lomonosov Moscow State University, Moscow 119991, Russia;* orcid.org/0000-0003-4708-6895

Complete contact information is available at: https://pubs.acs.org/10.1021/acsphotonics.0c01759

Notes

The authors declare no competing financial interest.

https://dx.doi.org/10.1021/acsphotonics.0c01759
ACS Photonics 2021, 8, 824−831

■ ACKNOWLEDGMENTS

The work was performed under financial support of the Russian Ministry of Education and Science (Grant No. 14.W03.31.0008), Russian Science Foundation (Grant No. 20-12-00371, nonlinear-optical measurements), Australian Research Council (DE180100070 and DP180100077), and the University of Technology Sydney (Seed Funding Grant). Part of the research was supported by MSU Quantum Technology Centre. A.A.P. acknowledges support by Foundation for the Advancement of Theoretical Physics and Mathematics "BASIS" (Grant No. 19-2-6-28-1). I.M.A. thanks Russian Foundation for Basic Research (Grant No. 19-02-00876, solid-state sample characterization). I.A. gratefully acknowledges the Australian Research council (CE200100010) and the Asian Office of Aerospace Research and Development (FA2386-20-1-4014).

■ REFERENCES

(1) Susarla, S.; Kutana, A.; Hachtel, J. A.; Kochat, V.; Apte, A.; Vajtai, R.; Idrobo, J. C.; Yakobson, B. I.; Tiwary, C. S.; Ajayan, P. M. Quaternary 2D transition metal dichalcogenides (TMDs) with tunable bandgap. *Adv. Mater.* **2017**, *29*, 1702457.

(2) Dawlaty, J. M.; Shivaraman, S.; Chandrashekhar, M.; Rana, F.; Spencer, M. G. Measurement of ultrafast carrier dynamics in epitaxial graphene. *Appl. Phys. Lett.* **2008**, *92*, 042116.

(3) Yuan, L.; Wang, T.; Zhu, T.; Zhou, M.; Huang, L. Exciton dynamics, transport, and annihilation in atomically thin two-dimensional semiconductors. *J. Phys. Chem. Lett.* **2017**, *8*, 3371−3379.

(4) Chen, Y.; Xi, J.; Dumcenco, D. O.; Liu, Z.; Suenaga, K.; Wang, D.; Shuai, Z.; Huang, Y.-S.; Xie, L. Tunable band gap photoluminescence from atomically thin transition-metal dichalcogenide alloys. *ACS Nano* **2013**, *7*, 4610−4616.

(5) Ma, C.; Wang, C.; Gao, B.; Adams, J.; Wu, G.; Zhang, H. Recent progress in ultrafast lasers based on 2D materials as a saturable absorber. *Appl. Phys. Rev.* **2019**, *6*, 041304.

(6) Cassabois, G.; Valvin, P.; Gil, B. Hexagonal boron nitride is an indirect bandgap semiconductor. *Nat. Photonics* **2016**, *10*, 262−266.

(7) Watanabe, K.; Taniguchi, T.; Niiyama, T.; Miya, K.; Taniguchi, M. Far-ultraviolet plane-emission handheld device based on hexagonal boron nitride. *Nat. Photonics* **2009**, *3*, 591.

(8) Watanabe, K.; Taniguchi, T.; Kanda, H. Direct-bandgap properties and evidence for ultraviolet lasing of hexagonal boron nitride single crystal. *Nat. Mater.* **2004**, *3*, 404−409.

(9) Zhi, C.; Bando, Y.; Tang, C.; Kuwahara, H.; Golberg, D. Large-scale fabrication of boron nitride nanosheets and their utilization in polymeric composites with improved thermal and mechanical properties. *Adv. Mater.* **2009**, *21*, 2889−2893.

(10) Li, L. H.; Cervenka, J.; Watanabe, K.; Taniguchi, T.; Chen, Y. Strong oxidation resistance of atomically thin boron nitride nanosheets. *ACS Nano* **2014**, *8*, 1457−1462.

(11) Krasheninnikov, A.; Nordlund, K. Ion and electron irradiation-induced effects in nanostructured materials. *J. Appl. Phys.* **2010**, *107*, 071301.

(12) Lee, K. H.; Shin, H.-J.; Lee, J.; Lee, I.-Y.; Kim, G.-H.; Choi, J.-Y.; Kim, S.-W. Large-scale synthesis of high-quality hexagonal boron nitride nanosheets for large-area graphene electronics. *Nano Lett.* **2012**, *12*, 714−718.

(13) Bresnehan, M. S.; Hollander, M. J.; Wetherington, M.; LaBella, M.; Trumbull, K. A.; Cavalero, R.; Snyder, D. W.; Robinson, J. A. Integration of hexagonal boron nitride with quasi-freestanding epitaxial graphene: toward wafer-scale, high-performance devices. *ACS Nano* **2012**, *6*, 5234−5241.

(14) Gupta, A.; Sakthivel, T.; Seal, S. Recent development in 2D materials beyond graphene. *Prog. Mater. Sci.* **2015**, *73*, 44−126.

(15) Wang, J.; Ma, F.; Liang, W.; Wang, R.; Sun, M. Optical, photonic and optoelectronic properties of graphene, h-BN and their hybrid materials. *Nanophotonics* **2017**, *6*, 943−976.

(16) Cui, X.; Lee, G.-H.; Kim, Y. D.; Arefe, G.; Huang, P. Y.; Lee, C.-H.; Chenet, D. A.; Zhang, X.; Wang, L.; Ye, F.; et al. Multi-terminal transport measurements of MoS_2 using a van der Waals heterostructure device platform. *Nat. Nanotechnol.* **2015**, *10*, 534−540.

(17) Wu, S.; Fatemi, V.; Gibson, Q. D.; Watanabe, K.; Taniguchi, T.; Cava, R. J.; Jarillo-Herrero, P. Observation of the quantum spin Hall effect up to 100 kelvin in a monolayer crystal. *Science* **2018**, *359*, 76−79.

(18) Uchiyama, Y.; Kutana, A.; Watanabe, K.; Taniguchi, T.; Kojima, K.; Endo, T.; Miyata, Y.; Shinohara, H.; Kitaura, R. Momentum-forbidden dark excitons in hBN-encapsulated monolayer MoS_2. *NPJ. 2D Mater. Appl.* **2019**, *3*, 26.

(19) Caldwell, J. D.; Kretinin, A. V.; Chen, Y.; Giannini, V.; Fogler, M. M.; Francescato, Y.; Ellis, C. T.; Tischler, J. G.; Woods, C. R.; Giles, A. J.; et al. Sub-diffractional volume-confined polaritons in the natural hyperbolic material hexagonal boron nitride. *Nat. Commun.* **2014**, *5*, 5221.

(20) Tran, T. T.; Bray, K.; Ford, M. J.; Toth, M.; Aharonovich, I. Quantum emission from hexagonal boron nitride monolayers. *Nat. Nanotechnol.* **2016**, *11*, 37−41.

(21) Kumar, R.; Sahoo, S.; Joanni, E.; Singh, R. K.; Yadav, R. M.; Verma, R. K.; Singh, D. P.; Tan, W. K.; Perez del Pino, A.; Moshkalev, S. A.; Matsuda, A. A review on synthesis of graphene, h-BN and MoS_2 for energy storage applications: Recent progress and perspectives. *Nano Res.* **2019**, *12*, 2655−2694.

(22) Kim, S.; Fröch, J. E.; Christian, J.; Straw, M.; Bishop, J.; Totonjian, D.; Watanabe, K.; Taniguchi, T.; Toth, M.; Aharonovich, I. Photonic crystal cavities from hexagonal boron nitride. *Nat. Commun.* **2018**, *9*, 2623.

(23) Fröch, J. E.; Kim, S.; Mendelson, N.; Kianinia, M.; Toth, M.; Aharonovich, I. Coupling hexagonal boron nitride quantum emitters to photonic crystal cavities. *ACS Nano* **2020**, *14*, 7085−7091.

(24) Li, Y.; Rao, Y.; Mak, K. F.; You, Y.; Wang, S.; Dean, C. R.; Heinz, T. F. Probing symmetry properties of few-layer MoS_2 and h-BN by optical second-harmonic generation. *Nano Lett.* **2013**, *13*, 3329−3333.

(25) Kim, C.-J.; Brown, L.; Graham, M. W.; Hovden, R.; Havener, R. W.; McEuen, P. L.; Muller, D. A.; Park, J. Stacking order dependent second harmonic generation and topological defects in h-BN bilayers. *Nano Lett.* **2013**, *13*, 5660−5665.

(26) Kim, S.; Fröch, J. E.; Gardner, A.; Li, C.; Aharonovich, I.; Solntsev, A. S. Second-harmonic generation in multilayer hexagonal boron nitride flakes. *Opt. Lett.* **2019**, *44*, 5792−5795.

(27) Smirnova, D. A.; Solntsev, A. S. Cascaded third-harmonic generation in hybrid graphene-semiconductor waveguides. *Phys. Rev. B: Condens. Matter Mater. Phys.* **2015**, *92*, 155410.

(28) Bernhardt, N.; Koshelev, K.; White, S. J.; Meng, K. W. C.; Fröch, J. E.; Kim, S.; Tran, T. T.; Choi, D.-Y.; Kivshar, Y.; Solntsev, A. S. Quasi-BIC resonant enhancement of second-harmonic generation in WS_2 monolayers. *Nano Lett.* **2020**, *20*, 5309−5314.

(29) Taniguchi, T.; Watanabe, K. Synthesis of high-purity boron nitride single crystals under high pressure by using Ba-BN solvent. *J. Cryst. Growth* **2007**, *303*, 525−529.

(30) Desai, S. B.; Madhvapathy, S. R.; Amani, M.; Kiriya, D.; Hettick, M.; Tosun, M.; Zhou, Y.; Dubey, M.; Ager, J. W., III; Chrzan, D.; et al. Gold-mediated exfoliation of ultralarge optoelectronically-perfect monolayers. *Adv. Mater.* **2016**, *28*, 4053−4058.

(31) Akhmanov, S. A.; Vysloukh, V. A.; Chirkin, A. S. *Optics of Femtosecond Laser Pulses*; AIP: New York, 1992.

(32) Michel, K.; Verberck, B. Phonon dispersions and piezoelectricity in bulk and multilayers of hexagonal boron nitride. *Phys. Rev. B: Condens. Matter Mater. Phys.* **2011**, *83*, 115328.

(33) Jiang, T.; Huang, D.; Cheng, J.; Fan, X.; Zhang, Z.; Shan, Y.; Yi, Y.; Dai, Y.; Shi, L.; Liu, K.; et al. Gate-tunable third-order nonlinear optical response of massless Dirac fermions in graphene. *Nat. Photonics* **2018**, *12*, 430−436.

(34) Schubert, M.; Rheinländer, B.; Franke, E.; Neumann, H.; Hahn, J.; Röder, M.; Richter, F. Anisotropy of boron nitride thin-film

https://dx.doi.org/10.1021/acsphotonics.0c01759
ACS Photonics 2021, 8, 824−831

reflectivity spectra by generalized ellipsometry. *Appl. Phys. Lett.* **1997**, *70*, 1819−1821.
(35) Bethune, D. Optical harmonic generation and mixing in multilayer media: analysis using optical transfer matrix techniques. *J. Opt. Soc. Am. B* **1989**, *6*, 910−916.
(36) Rodríguez, C.; Rudolph, W. Modeling third-harmonic generation from layered materials using nonlinear optical matrices. *Opt. Express* **2014**, *22*, 25984−25992.
(37) Martemyanov, M. G.; Kim, E. M.; Dolgova, T. V.; Fedyanin, A. A.; Aktsipetrov, O. A.; Marowsky, G. Third-harmonic generation in silicon photonic crystals and microcavities. *Phys. Rev. B: Condens. Matter Mater. Phys.* **2004**, *70*, 073311.
(38) Afinogenov, B. I.; Popkova, A. A.; Bessonov, V. O.; Lukyanchuk, B.; Fedyanin, A. A. Phase matching with Tamm plasmons for enhanced second-and third-harmonic generation. *Phys. Rev. B: Condens. Matter Mater. Phys.* **2018**, *97*, 115438.
(39) Shen, Y. Optical second harmonic generation at interfaces. *Annu. Rev. Phys. Chem.* **1989**, *40*, 327−350.
(40) Rosa, H. G.; Ho, Y. W.; Verzhbitskiy, I.; Rodrigues, M. J.; Taniguchi, T.; Watanabe, K.; Eda, G.; Pereira, V. M.; Gomes, J. C. Characterization of the second-and third-harmonic optical susceptibilities of atomically thin tungsten diselenide. *Sci. Rep.* **2018**, *8*, 10035.
(41) Bloembergen, N.; Pershan, P. Light waves at the boundary of nonlinear media. *Phys. Rev.* **1962**, *128*, 606.
(42) Gubler, U.; Bosshard, C. Optical third-harmonic generation of fused silica in gas atmosphere: Absolute value of the third-order nonlinear optical susceptibility $\chi^{(3)}$. *Phys. Rev. B: Condens. Matter Mater. Phys.* **2000**, *61*, 10702.
(43) Wang, R.; Chien, H.-C.; Kumar, J.; Kumar, N.; Chiu, H.-Y.; Zhao, H. Third-harmonic generation in ultrathin films of MoS_2. *ACS Appl. Mater. Interfaces* **2014**, *6*, 314−318.
(44) Chelikowsky, J. R.; Cohen, M. L. Nonlocal pseudopotential calculations for the electronic structure of eleven diamond and zinc-blende semiconductors. *Phys. Rev. B* **1976**, *14*, 556.
(45) Hong, S.-Y.; Dadap, J. I.; Petrone, N.; Yeh, P.-C.; Hone, J.; Osgood Jr., R. M. Optical third-harmonic generation in graphene. *Phys. Rev. X* **2013**, *3*, 021014.
(46) Autere, A.; Jussila, H.; Marini, A.; Saavedra, J.; Dai, Y.; Säynätjoki, A.; Karvonen, L.; Yang, H.; Amirsolaimani, B.; Norwood, R. A.; et al. Optical harmonic generation in monolayer group-VI transition metal dichalcogenides. *Phys. Rev. B: Condens. Matter Mater. Phys.* **2018**, *98*, 115426.
(47) Burns, W.; Bloembergen, N. Third-harmonic generation in absorbing media of cubic or isotropic symmetry. *Phys. Rev. B* **1971**, *4*, 3437.
(48) Ning, T.; Hyvärinen, O.; Pietarinen, H.; Kaplas, T.; Kauranen, M.; Genty, G. Third-harmonic UV generation in silicon nitride nanostructures. *Opt. Express* **2013**, *21*, 2012−2017.
(49) Malitson, I. H. Interspecimen comparison of the refractive index of fused silica. *J. Opt. Soc. Am.* **1965**, *55*, 1205−1209.
(50) Sutherland, R. L. *Handbook of Nonlinear Optics*, 1st ed.; Marcel Dekker, Inc.: New York, 1996.
(51) Woodward, R.; Murray, R.; Phelan, C.; De Oliveira, R.; Runcorn, T.; Kelleher, E.; Li, S.; De Oliveira, E.; Fechine, G.; Eda, G.; De Matos, C. Characterization of the second-and third-order nonlinear optical susceptibilities of monolayer MoS_2 using multiphoton microscopy. *2D Mater.* **2017**, *4*, 011006.
(52) Yang, X.-L.; Xie, S.-W. Expression of third-order effective nonlinear susceptibility for third-harmonic generation in crystals. *Appl. Opt.* **1995**, *34*, 6130−6135.
(53) Miller, R. C. Optical second harmonic generation in piezoelectric crystals. *Appl. Phys. Lett.* **1964**, *5*, 17−19.
(54) Boyd, R. W. *Nonlinear Optics*, 2nd ed.; Academic Press: New York, 2003.
(55) Ettoumi, W.; Petit, Y.; Kasparian, J.; Wolf, J.-P. Generalized Miller formulæ. *Opt. Express* **2010**, *18*, 6613−6620.

https://dx.doi.org/10.1021/acsphotonics.0c01759
ACS Photonics 2021, 8, 824−831